



Contents lists available at SciVerse ScienceDirect

## Computational Materials Science

journal homepage: [www.elsevier.com/locate/commatsci](http://www.elsevier.com/locate/commatsci)

## A reactive force-field for Zirconium and Hafnium Di-Boride

Aff Gousssem<sup>a</sup>, Wu Fan<sup>a</sup>, Adri C.T. van Duin<sup>c</sup>, Pradeep Sharma<sup>a,b,\*</sup><sup>a</sup> Department of Mechanical Engineering, University of Houston, Cullen College of Engineering, Engineering Building 1, Houston, TX 77204, USA<sup>b</sup> Department of Physics, University of Houston, 617 Science & Research Building 1, Houston, TX 77204, USA<sup>c</sup> Department of Mechanical and Nuclear Engineering, Pennsylvania State University, 136 Research East Building, University Park, PA 16802, USA

## ARTICLE INFO

## Article history:

Received 11 September 2012

Received in revised form 2 December 2012

Accepted 17 December 2012

## Keywords:

Interatomic force-field

Chemical reactions

High temperature materials

## ABSTRACT

Zirconium and Hafnium Di-Boride are the two major material systems that are of critical importance for applications in ultra-high temperature environments where both oxidation and mechanical damage mechanisms (such as creep) are operative. Atomistic simulations of these materials at finite temperatures have been hampered due to the unavailability of inter-atomic potentials for the involved elements. In this paper, we present the development of interatomic potentials for both  $ZrB_2$  and  $HfB_2$  within the ReaxFF framework—thus enabling modeling of chemical reactions. The parameters of the reactive force field are derived by fitting to detailed quantum mechanical simulations of  $ZrB_2$  and  $HfB_2$  clusters and crystal structures.

© 2013 Elsevier B.V. All rights reserved.

## 1. Introduction

The aim of this study is to develop transferable reactive force fields for Zirconium and Hafnium Di-Boride.  $ZrB_2$  and  $HfB_2$  are emerging Ultra High Temperature Ceramics (UHTCs) with a relatively low density (6.09 g/cm<sup>3</sup> and 11.09 g/cm<sup>3</sup>), high melting point (around 3300 K), and high elastic modulus (around 450 GPa). These excellent and unique combinations of properties make them highly desirable candidates for numerous applications requiring high thermal and mechanical resistance [1–5]. Hypersonic flights, rocket propulsion systems, thermal protection for space vehicles, present – for instance – perfect environments where  $ZrB_2$  (and Hf and Ta borides as well) can exhibit an advantage [6]. The leading and trailing edges of wing and several other components require such robust materials that are reliable at these high temperatures. The outstanding physical stability of  $ZrB_2$  can be explained partly by the employment of pressure-assisted sintering techniques at a very high temperatures (>2200 K) [7–9], and to the doping with ceramic-type additives (silicon carbide, silicon nitride, etc.) [10,11] which could – in some cases – enhance properties such as hardness, fracture toughness, strength, and resistance to oxidation.

In order to study and predict the behavior of these materials, and the possible interactions with different additives or external agents, the development of an inter-atomic potential model is critical. Among the several types of inter-atomic interaction models,

the so-called Reax Force Field (ReaxFF) framework appears to be a good choice. Reactive force field potentials are able to accurately model chemical reactions including breaking and reforming dynamics of bonds [12–14]. Furthermore, void nucleation, void growth, diffusion-based processes such as grain boundary sliding, oxidation among others are some of the phenomena that are likely targets of future atomistic modeling. All these require accurate handling of bond formation, disassociation, and charge-redistribution at finite temperatures. ReaxFF approach has been shown in past work to accurately account for these aspects [12–14].

The development of Reax potentials requires the fitting of a large number of parameters to quantum mechanical (QM) calculations. This parameterization can be done using the following procedure:

- (i) Establish the relevant terms necessary for the given material in the total energy expression of the functional form of the interatomic potential.
- (ii) Create a training set of data points through QM calculations (mainly energies and charge distribution).
- (iii) Fit the parameters using the training set.
- (iv) Validate the obtained parameters by comparing molecular dynamics (MD) results using the obtained potential to either experimental or QM results.

The outline of the paper is as follows: in Section 2, we describe the general ReaxFF approach, QM calculations are presented in Section 3 while we outline the fitting and optimization process in Section 4. Finally, in Section 5 we present results of MD simulations using the obtained potential to illustrate its capabilities.

\* Corresponding author at: Department of Mechanical Engineering, University of Houston, Cullen College of Engineering, Engineering Building 1, Houston, TX 77204, USA.

E-mail address: [psharma@uh.edu](mailto:psharma@uh.edu) (P. Sharma).

## 2. ReaxFF overview

The basic concept underpinning the creation of any interatomic potential is to find the adequate parameters in the energy expression that fit QM or experimental data points and well-replicate some selected physical properties. Unlike most interatomic potentials in use for metals or ceramics, in the ReaxFF, the energy expression depends on the bond order in addition to the usual bond distances, angles, etc. Bond orders describe the number of electrons shared between two atoms as a non-integer function of the distance separating them. This is the key point that allows the reactive potential to accurately model bond breaking/formation, and then, reaction paths. In addition to this, the charge distribution is a continuous function of atom spacing; and is updated at every iteration of an atomistic simulation.

The bond order associated with two atoms  $i$  and  $j$  is given by [15]:

$$BO'_{ij} = \exp \left[ p_{bo1} \cdot \left( \frac{r_{ij}}{r_0^\sigma} \right)^{p_{bo2}} \right] + \exp \left[ p_{bo3} \cdot \left( \frac{r_{ij}}{r_0^\pi} \right)^{p_{bo4}} \right] + \exp \left[ p_{bo5} \cdot \left( \frac{r_{ij}}{r_0^{\pi\pi}} \right)^{p_{bo6}} \right] \quad (1)$$

where  $r_0^\sigma$ ,  $r_0^\pi$ ,  $r_0^{\pi\pi}$  are the bond radii of  $\sigma$ ,  $\pi$ , and  $\pi\pi$  bonds and  $p_{bo1-6}$  are the bond order parameters. In  $ZrB_2$  and  $HfB_2$  structures,  $\pi$  and  $\pi\pi$  contributions are not relevant.

In order to remove the unrealistic weak bonds between normally coordinated atoms and their next neighbors, a bond order correction algorithm is used. The bond orders are, then, allowed to be adjusted by the ReaxFF algorithm.

The total interaction energy expression for ReaxFF is given in the most general case by [15]:

$$E_{total} = E_{bond} + E_{val} + E_{tors} + E_{over} + E_{under} + E_{pen} + E_{lp} + E_{conj} + E_{vdw} + E_{coulomb} \quad (2)$$

where the contributions of the different forms of energy depend on the bond order and are either bonded interaction terms: Bond energy ( $E_{bond}$ ), valence energy ( $E_{val}$ ), torsion energy ( $E_{tors}$ ), over-coordination (respectively under-coordination), penalty energy ( $E_{over}$  respectively  $E_{under}$ ), lone pair energies ( $E_{lp}$ ), conjugated bond energies ( $E_{conj}$ ), energy penalty for handling atoms with two double bonds ( $E_{pen}$ ) or non-bonded interaction terms: van der Waals energy ( $E_{vdw}$ ) and Coulomb energy ( $E_{coulomb}$ ).

A detailed description of the expressions and significance of these terms can be found in [15]. In the context of  $ZrB_2$  and  $HfB_2$ , some of these terms can be ignored, reducing the energy expression to the following equation:

$$E_{total} = E_{bond} + E_{val} + E_{over} + E_{vdw} + E_{coulomb} \quad (3)$$

## 3. QM calculations and training set

The quantum-mechanical calculations were performed using the Quantumwise program [16] for periodic crystal phase and GAUSSIAN09 program for the geometrical optimization and potential energy curves for  $Zr(BH_2)_2$  and  $Hf(BH_2)_2$ . QM calculations were performed for  $ZrB_2$  (respectively  $HfB_2$ ) in a hexagonally closed packed structure with lattice parameters  $a = 3.22 \text{ \AA}$ ,  $c = 3.54 \text{ \AA}$  (respectively  $a = 3.14 \text{ \AA}$ ,  $c = 3.47 \text{ \AA}$ ).

To ensure “reasonable” transferability, the training set should be sufficiently large to characterize material properties of interest. Our training set contains a set of five types of simulations: elastic constants, charge distribution, heat of formation, equation of state, and surface energy.

### 3.1. Elastic constants

When subjected to sufficiently small strains, the crystal deforms in a linear elastic manner (Eq. (4)). A good parameterization of elastic constants is critical for accurate calculation of defect energies and thermal properties. The elastic constants  $C_{ijkl}$  are the derivatives of the elastic energy density with respect to the strain tensor. By applying the strain in specific directions, most of the terms in (Eq. (4)) vanish. The energy expression can be simplified to (Eq. (5)) where  $\mathbf{A}$  is defined in Fig. 1.

$$E(V, \varepsilon) = E_0 + V_0 \sum_{i,j,k,l} \frac{1}{2} C_{ijkl} \varepsilon_{ij} \varepsilon_{kl} \quad (4)$$

$$E(V, \varepsilon) = E_0 + \frac{V_0}{2} A \delta^2 \quad (5)$$

By means of polynomial fit of the total energy versus strain, the elastic constants can be extracted. To do so, we define the lattice of HCP  $ZrB_2$  by a set a three primitive Bravice lattice vectors  $\mathbf{R}$  (Eq. (6)). The vectors of the deformed lattice  $\mathbf{R}'$  can be obtained by  $\mathbf{R}' = \mathbf{D}\mathbf{R}$ , where  $\mathbf{D}$  is defined in terms of the strain tensor elements  $\varepsilon_{ij}$  (Eq. (7)):

$$R = \begin{bmatrix} a/2 & a\sqrt{3}/2 & 0 \\ a/2 & a\sqrt{3}/2 & 0 \\ 0 & 0 & c \end{bmatrix} \quad (6)$$

$$D = \begin{bmatrix} 1 + \varepsilon_{11} & \varepsilon_{12} & \varepsilon_{13} \\ \varepsilon_{21} & 1 + \varepsilon_{22} & \varepsilon_{23} \\ \varepsilon_{31} & \varepsilon_{32} & 1 + \varepsilon_{33} \end{bmatrix} \quad (7)$$

By applying different distortion matrices, the complete elasticity tensor can be populated. For HCP materials, only five unique distortions are needed to construct the elasticity tensor. Fig. 1 presents our results for this calculation.

The computational cells consisted of super-cells of hexagonal  $ZrB_2$  and  $HfB_2$  with 24 atoms (eight unit cells). The DFT calculations were performed using the generalized gradient approximation (GGA), the plane wave energy cutoff was set to 1500 eV, and the system was sampled using  $4 \times 4 \times 4$   $k$ -points. These parameters ensured a convergence of the total energy of the cell within 0.04 eV.

The elastic constants for both materials are presented in Table 1. A comparison with present experimental data [17] is also presented.

### 3.2. Surface energy

Surface energy is an important property from a parameterization perspective. Accurate modeling of surface energy allows a more faithful accounting of melting temperature, fracture behavior, chemical reactions (which often occur at surfaces), defect energies, void formation, etc. The surface energy is defined as the energy required to create a unit of surface area (Eq. (8)).

For that purpose two geometries were used for each material: a 3D periodic  $ZrB_2$  (respectively  $HfB_2$ ) bulk with 12 atoms super-cell and total energy  $E_0$ . The second structure consisted of a non-periodic system in the  $z$  direction with two free surfaces (top and bottom) endowed with a total energy of  $E_1$ .  $A$  is the area of the surface. The factor  $1/2$  accounts for the two surfaces of the slab. Then,

$$\gamma = \frac{1}{2A} (E_0 - E_1) \quad (8)$$

Through DFT calculations on the aforementioned configurations we find the (0001) surface energy of both  $ZrB_2$  and  $HfB_2$  respectively as  $\gamma = 1.6 \text{ J m}^{-2}$  and  $\gamma = 4.52 \text{ J m}^{-2}$ .

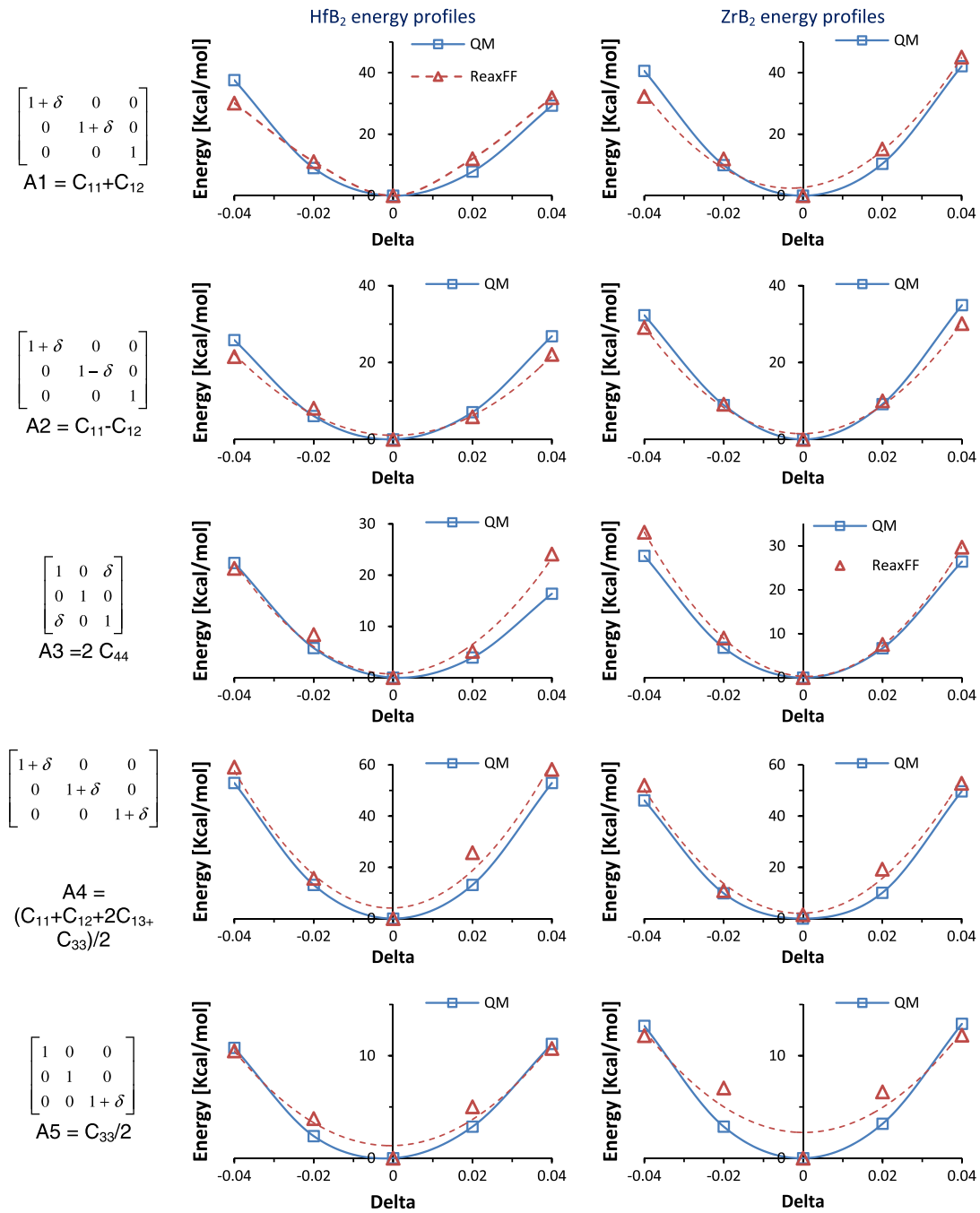


Fig. 1. Energy profiles for different distortion paths.

**Table 1**  
ZrB<sub>2</sub> and HfB<sub>2</sub> elastic constants (GPa).

		C11	C12	C13	C33	C44
HfB <sub>2</sub>	Experimental [17]	583.3	98.4	131.8	456.2	257.7
	DFT	592.2	101.3	134.0	449.1	267.6
ZrB <sub>2</sub>	Experimental [17]	581.0	55.0	121.0	445.0	240.0
	DFT	589.6	66.4	118.2	438.4	248.2

### 3.3. Mulliken charge distribution

Mulliken population analysis provides a mean of estimating partial atomic charges. It can have, for some systems, a crucial role in determining the reaction paths. For that reason, special care

is given to Mulliken population analysis for both bulk and surface. Two samples are investigated for each material: a 3D periodic crystal, and an infinite sheet of four layers. By including both simulations in the training set, we emphasize the effect of the free surfaces.

**Table 2**  
Charge distribution for ZrB<sub>2</sub> and HfB<sub>2</sub> samples.

Atom	Type	ZrB <sub>2</sub>		HfB <sub>2</sub>	
		Sheet	Bulk	Sheet	Bulk
1	Type	+0.3392	+0.6995	+0.2302	+0.4751
2	Zr/Hf	+0.5895	+0.6984	+0.4001	+0.4746
3	Zr/Hf	+0.6667	+0.6992	+0.4525	+0.4739
4	Zr/Hf	+0.3475	+0.6984	+0.2353	+0.4746
5	Zr/Hf	-0.2996	-0.3496	-0.2033	-0.2374
6	B	-0.3374	-0.3492	-0.2290	-0.2371
7	B	-0.3310	-0.3494	-0.2247	-0.2371
8	B	-0.0034	-0.3493	-0.0023	-0.2374
9	B	-0.2996	-0.3494	-0.2033	-0.2374
10	B	-0.3374	-0.3496	-0.2290	-0.2371
11	B	-0.3310	-0.3495	-0.2247	-0.2371
12	B	-0.0034	-0.3496	-0.0021	-0.2374

The QM charge distribution calculation results are presented in Table 2.

### 3.4. Bond dissociation

Fitting the bond dissociation curves of HfB<sub>2</sub> and ZrB<sub>2</sub> is important in the determination of the correct parameters for the bond order and bond order correction values since these provide the basis for the “energy vs. bond length” and “energy vs. angle” curves. The bond dissociation curves were obtained by varying the **Zr–B** and **Hf–B** bond lengths from 1.3 Å to 5.5 Å (Fig. 2a and c). GAUSSIAN09 software was used to obtain single point energies for the different structures. The change of the molecules energy with respect to the main angles (**B–Zr–B** and **B–Hf–B**) was also investigated: angles were varied by 40° around the equilibrium (Fig. 2b and d). Because of the instability of ZrB<sub>2</sub> and HfB<sub>2</sub> molecules during the QM calculations, hydrogen saturated atoms were used: Zr(BH<sub>2</sub>)<sub>2</sub> and Hf(BH<sub>2</sub>)<sub>2</sub> single point energies were then extrapolated to obtain Fig. 2a–d.

### 4. Parameterization procedure

To obtain reliable estimates of any physical property using the ReaxFF potential, it is important to fit the potential as closely as possible to the QM and experimental training set. The parameterization of the potential consists of the following steps:

- (i) An extended training set data containing 104 data points for each material is generated for both ZrB<sub>2</sub> and HfB<sub>2</sub> crystals, and Zr(BH<sub>2</sub>)<sub>2</sub> and Hf(BH<sub>2</sub>)<sub>2</sub> molecules. Six main types of QM and experimental data were added to the training set:
  - **Mulliken charge distribution:** charge distributions for both periodic and non-periodic crystals were computed [24 data points].
  - **Elastic constants:** a total of five energy vs. strain curves for different applied strains were obtained and the elasticity tensor was computed [36 data points].
  - **Gas phase dissociation curve:** a total of 20 data points were added to extrapolate the bond dissociation curve and the dependence of the molecule energy with the central angle.
  - **Equations of state:** three equations of states were developed for each material; homogenous expansion, expansion in (0001) plane, and expansion in <0001> direction [15 data points].
  - **Surface energy:** (0001) surface energy was calculated and added to the training set [two data points].
  - **Heat of formation:** formation energies for both ZrB<sub>2</sub> and HfB<sub>2</sub> crystals were added to the training set [one data point].
  - **Intrinsic defect energies:** experimental results on Zr, B, and ZrB<sub>2</sub> intrinsic defect energies were available. However, QM calculations were performed to obtain defect energies for Hf, B and HfB<sub>2</sub>. These data points have been added to the training set as well [six data points].
- (ii) Energy contribution from torsion, penalty, lone pairing, and conjugation were neglected in order to reduce the number of parameters. A total of 44 parameters were selected.

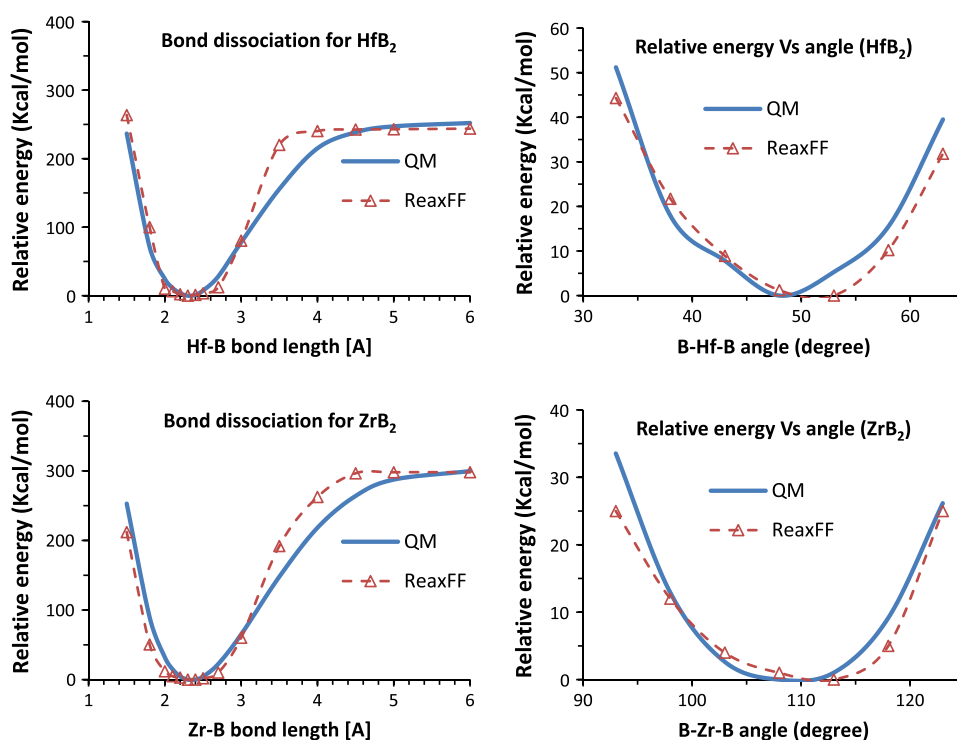


Fig. 2. Bond length and angle effect on energy profiles for ZrB<sub>2</sub> and HfB<sub>2</sub>.

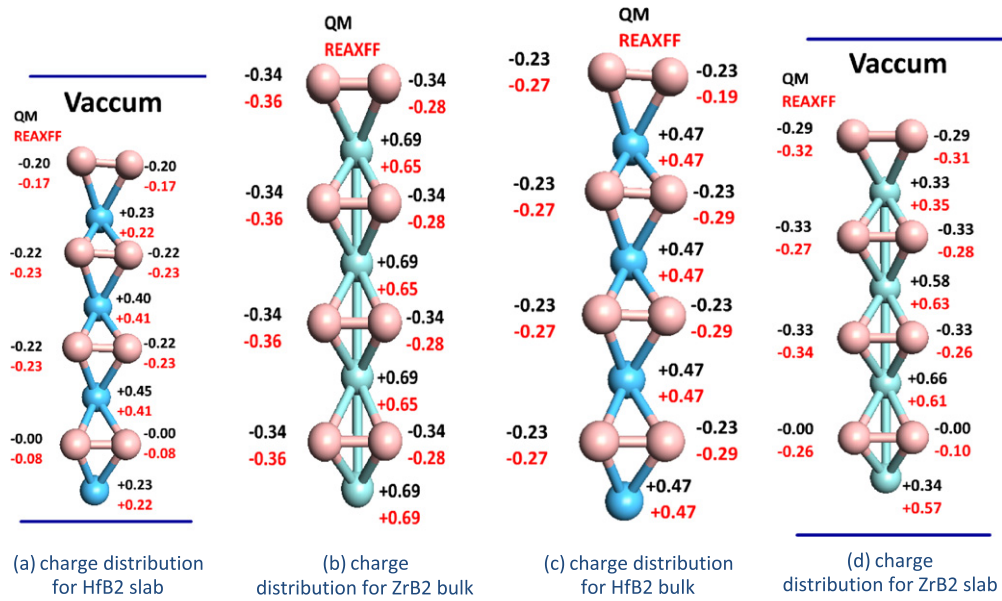


Fig. 3. Mulliken charge distribution for  $ZrB_2$  and  $HfB_2$ .

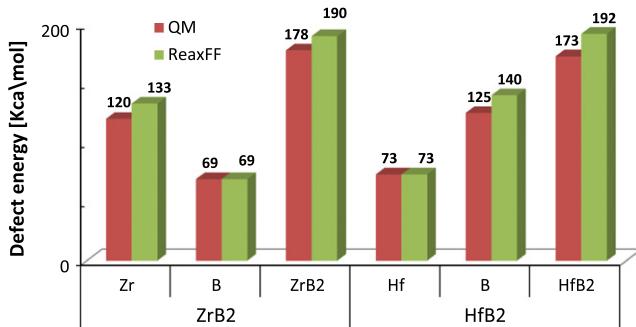


Fig. 4. Intrinsic defect energies for  $ZrB_2$  and  $HfB_2$ .

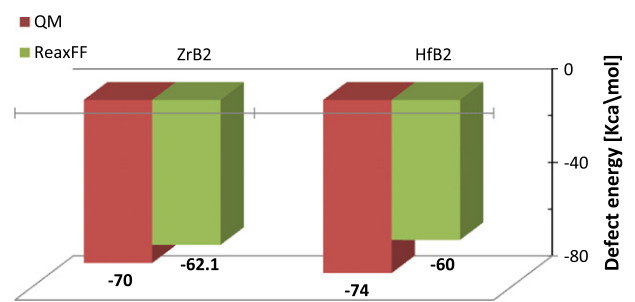


Fig. 6.  $ZrB_2$  and  $HfB_2$  heat of formation energies.

- (iii) The parameters were fitted to the generated training set using a custom-in-house optimization program.
- (iv) The potential parameters were validated by comparison of the force-field base molecular dynamics to QM and experimental results.

Our final optimized parameters are listed in Tables a–e (Appendix) and a comparison between DFT and fitted results are presented in Figs. 3–6.

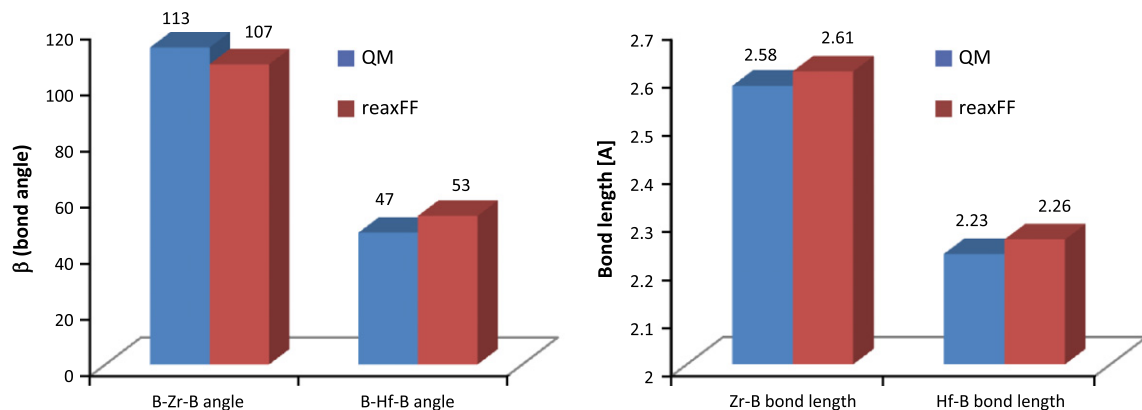


Fig. 5. Molecular properties for  $ZrB_2$  and  $HfB_2$ .

## 5. Application: ion bombardment

ReaxFF is a reactive empirical bond order potential that is able to model the formation and dissociation of bonds by using the bond order concept. It has been parameterized to model atomic reactions. Thus, in order to illustrate the potential and investigate its ability to capture physical phenomena that are not included in the training set, we performed MD simulations of ion-bombardment—specifically, Boron bombardment on Zr crystal.

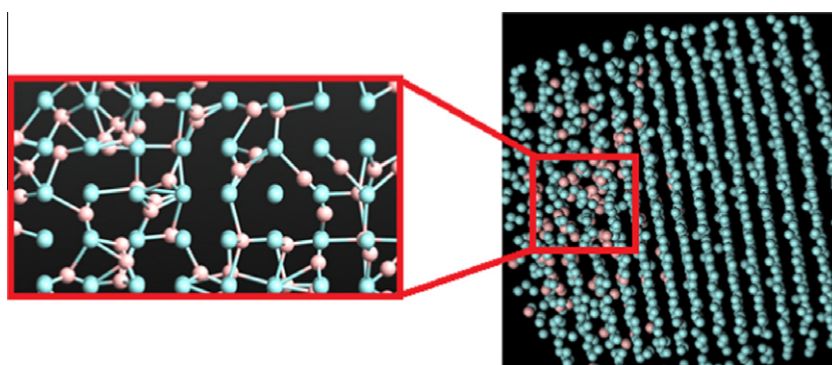


Fig. 7. (a and b) Snapshot of the samples after the atom bombardment. With originally no B–Zr connectivity, the defined potential was able to create atom connections.

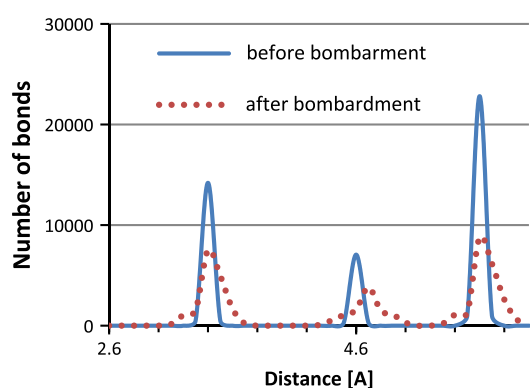


Fig. 8. Radial distribution function for pure Zr bulk (solid) and Zr bulk after B bombardment (dashed).

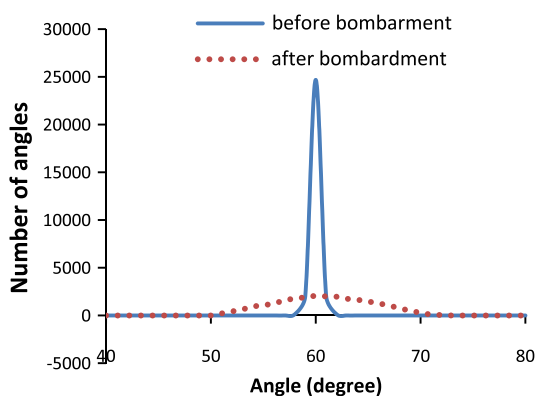


Fig. 9. Bond angle distribution for pure Zr bulk (solid) and Zr bulk after B bombardment (dashed).

The sample geometry was:  $32 \text{ \AA} \times 32 \text{ \AA} \times 32 \text{ \AA}$  (1372 atoms) for Zr bulk. A beam of B was bombarded at room temperature onto the Zr bulk. A total of 200 B atoms were bombarded with a velocity of  $2 \times 10^{14} \text{ \AA/s}$  and a time step of 0.2 fs (Fig. 7a).

Fig. 7b, which is an inset of the whole sample, illustrates clearly that the potential faithfully created atom connectivity between B and Zr atoms.

During the ion-bombardment process, the B atoms injected into the Zr crystal create a disordered state. Under “ideal” conditions, HCP structure of  $\text{ZrB}_2$  is expected in the regions of interaction. However, the kinetics of such a phase formation is very slow at room temperature. Therefore, during the ion-bombardment process, when the Zr matrix loses its cubic structure and is not able

to navigate the high-energy barriers to the HCP structure, a (meta-stable) amorphous state is induced.

A standard way to characterize the amorphous state is by tracking the changes in the radial distribution functions (RDFs), the bond angle distributions (BADs), and the average internal energy (U). A combination of these three analyses will confirm the creation of  $\text{ZrB}_2$  amorphous phase around the bombardment zone.

To investigate this further, we used the same sample (1372 Zr atoms with 200 B atoms). After the relaxation of the sample at room temperature, the average distances, angles, and energies are investigated.

### 5.1. RDF analysis

Fig. 8 clearly shows the presence of different peaks associated with first, second, and third neighbors that dominate the structure of the system. However, unlike a perfect crystal, close to the neighbor distances, some atoms are placed at non-ideal distances because of the injection of B interstitials into the bulk. The first neighbor is placed at 3.21 Å in the original structure and retains the same average configuration in the bombarded structure. However, a wider range of distances (3–3.5 Å) is observed. This confirms the presence of the  $\text{ZrB}_2$  amorphous phase.

### 5.2. BAD analysis

Investigation of the angle distribution reveals the same trend as the RDF analysis (Fig. 9). Since the bond angle distribution of an amorphous phase is different than that of a crystal phase by the presence of off-equilibrium angles (meta-stable states), the distributions are wider than for pure Zr.

### 5.3. Average internal energy analysis

Calculation of the internal energy of the system is another way to verify the amorphization of the material: internal energy for amorphous materials is in general higher than that of a crystalline material with the same number of atoms. During the MD simulation, the internal energy per atom increased from  $-74.12$  to  $-77.14$  kcal/mol. This increase is associated with the amorphization of the  $\text{ZrB}_2$  bulk.

## 6. Summary

We have developed a reactive force field for  $\text{ZrB}_2$  and  $\text{HfB}_2$  that will pave the way for accurate finite temperature atomistic simulations of these important ceramic compounds. A substantial training set of QM data for a wide variety of structures and energetic situations relevant to high temperature behavior of  $\text{ZrB}_2$  and

**Table a**  
General parameters.

<b>p_boc1</b>	<b>p_boc2</b>	<b>p_ovun3</b>	<b>p_ovun4</b>	<b>p_ovun6</b>
50.000	9.5469	50.000	0.6991	1.0500
<b>p_ovun7</b>	<b>p_ovun8</b>	<b>p_val7</b>	<b>p_val8</b>	<b>p_val9</b>
12.110	13.300	33.866	1.8512	1.0551
<b>p_val10</b>	<b>p_lp1</b>	<b>P_vdw1</b>	<b>R_tap</b>	<b>BO_cut_of</b>
2.0312	6.0891	1.5591	10.000	10.000

Bold fonts represent the name of the parameters and the “atom type/bond/angle”.

**Table b**  
Atom parameters.

	<b>r_cov1</b>	<b>r_cov2</b>	<b>r_cov3</b>	<b>p_boc3</b>	<b>p_boc4</b>
<b>Zr</b>	2.6214	−1.000	−1.000	0.1871	48.675
<b>Hf</b>	2.5612	−1.000	−1.000	0.2200	40.000
<b>B</b>	1.6690	−1.000	−1.000	6.0418	5.7491
	<b>p_boc5</b>	<b>D_vdw</b>	<b>valence</b>	<b>R_vdw</b>	<b>gamma_vdw</b>
<b>Zr</b>	0.0000	0.2201	4.0000	2.3435	47.463
<b>Hf</b>	0.0000	0.4112	4.0000	2.2931	30.510
<b>B</b>	1.0943	0.0050	3.0000	1.6500	2.3847
	<b>alpha_vdw</b>	<b>gamma_EEM</b>	<b>chi_EEM</b>	<b>eta_EEM</b>	
<b>Zr</b>	11.258	0.6797	1.5000	7.8552	
<b>Hf</b>	13.121	1.0000	1.2100	6.2530	
<b>B</b>	9.0923	1.0000	5.6220	7.4077	
	<b>p_ovun2</b>	<b>p_ovun5</b>	<b>p_val3</b>	<b>p_val5</b>	
<b>Zr</b>	−7.500	−5.000	3.3675	2.2600	
<b>Hf</b>	−6.127	−5.00000	2.413210	2.389700	
<b>B</b>	−2.859	0.1000	2.2695	2.8413	

Bold fonts represent the name of the parameters and the “atom type/bond/angle”.

**Table c**  
Bond parameters.

	<b>De_sigma</b>	<b>De_pi</b>	<b>De_pi_pi</b>	<b>p_be1</b>	<b>p_be2</b>	<b>p_bo1</b>
<b>Zr–Zr</b>	70.741	0.0000	0.0000	−0.2250	0.7347	−0.1076
<b>Hf–Hf</b>	89.224	0.0000	0.0000	0.2311	0.8771	−0.1101
<b>Zr–B</b>	168.46	0.0000	0.0000	0.1501	4.0000	−0.1351
<b>Hf–B</b>	162.76	0.0000	0.0000	0.3370	0.9640	−0.0987
<b>B–B</b>	74.532	0.0000	0.0000	0.9356	1.2112	−0.0840
	<b>p_bo2</b>	<b>p_bo3</b>	<b>p_bo4</b>	<b>p_bo5</b>	<b>p_bo6</b>	<b>p_ovun1</b>
<b>Zr–Zr</b>	7.3414	−0.200	15.000	−0.200	16.000	0.3872
<b>Hf–Hf</b>	6.2500	−0.200	15.000	−0.200	16.000	0.4412
<b>Zr–B</b>	8.5845	−0.200	15.000	−0.300	36.000	0.0100
<b>Hf–B</b>	9.3200	−0.200	15.000	−0.200	16.000	0.6130
<b>B–B</b>	7.5912	−0.200	15.000	−0.250	25.000	0.3446

Bold fonts represent the name of the parameters and the “atom type/bond/angle”.

HfB<sub>2</sub> clusters were used. Surface energies, heat of formations, defect energies, and charge distributions were also added to the training set to ensure that the obtained potential covers a vast area of physical phenomena. The surface and bulk energetics of the potential compare very well with density functional calculations. A simple ion-bombardment molecular dynamics simulation, predicated on the developed potential, confirmed the ability of the potential to model the formation and reaction of the expected bonds. An amorphous state was formed in the bombarded zone and was captured by means of radial distribution and bond angle distribution analysis.

**Table d**  
Valence parameters.

	<b>theta_o</b>	<b>p_val1</b>	<b>p_val2</b>	<b>p_val4</b>	<b>p_val7</b>
<b>Zr–Zr–Zr</b>	102.12	15.000	1.0000	1.0000	1.0000
<b>Zr–B–Zr</b>	90.000	13.091	6.2100	1.0000	1.1891
<b>B–Zr–Zr</b>	30.000	2.5000	1.0000	1.0000	1.0000
<b>B–B–Zr</b>	28.565	40.000	8.0000	1.0000	1.2394
<b>Zr–Zr–B</b>	46.290	15.630	4.9184	1.0000	1.5995
<b>B–Zr–B</b>	90.000	32.460	8.0000	1.0000	1.3478
<b>B–B–B</b>	72.956	15.870	3.4103	1.4129	1.3515
<b>Hf–Hf–Hf</b>	49.000	15.000	1.0000	1.0000	1.0000
<b>Hf–B–Hf</b>	32.000	11.000	5.6600	1.0000	1.1200
<b>B–Hf–Hf</b>	37.540	9.0000	1.0000	1.0000	1.0400
<b>B–B–Hf</b>	45.900	35.000	11.900	1.0000	1.4400
<b>Hf–Hf–B</b>	31.000	15.000	3.3200	1.0000	1.0100
<b>B–Hf–B</b>	58.000	27.000	8.0000	1.0000	1.5100

Bold fonts represent the name of the parameters and the “atom type/bond/angle”.

**Table e**  
Off-diagonal terms.

	<b>E_vdw</b>	<b>gamma_vdw</b>	<b>r_vdw</b>	<b>r_cov1</b>	<b>r_cov2</b>	<b>r_cov3</b>
<b>Zr–B</b>	0.1683	1.6183	10.7084	1.8503	−1.0000	−1.0000
<b>Hf–B</b>	0.3911	1.5912	16.3230	1.9213	−1.0000	−1.0000

Bold fonts represent the name of the parameters and the “atom type/bond/angle”.

## Acknowledgements

Sharma would like to acknowledge support from AFOSR Grant AFOSR FA9550-09-1-0200 (Program Manager: Ali Sayir). ACTvD gratefully acknowledge the support provided by the Air Force Office of Scientific Research (AFOSR) Grant No. FA9550-11-1-0158.

## Appendix A. Full set of parameters for ZrB<sub>2</sub> and HfB<sub>2</sub>

See Tables a–e.

## References

- [1] A.L. Chamberlain, W.G. Fahrenholtz, G.E. Hilmas, D.T. Ellerby, J. Amer. Ceram. Soc. 87 (2004) 1170.
- [2] F. Monteverde, A. Bellosi, J. Electromech. Soc. 150 (2003) B552.
- [3] F. Monteverde, A. Bellosi, S. Guicciardi, J. Eur. Ceram. Soc. 22 (2002) 279.
- [4] F. Peng, R.F. Speyer, J. Amer. Ceram. Soc. 91 (2008) 1489.
- [5] X.H. Zhang, P. Hu, J.C. Han, L. Xu, S.H. Meng, Scr. Mater. 57 (2007) 1036.
- [6] M. Tului, S. Lionetti, G. Pulci, F. Marra, J. Tirillò, T. Valente, Surf. Coat. Technol. 205 (2010) 1065.
- [7] A.L. Chamberlain, W.G. Fahrenholtz, G.E. Hilmas, J. Amer. Ceram. Soc. 89 (2006) 450.
- [8] A.L. Chamberlain, W.G. Fahrenholtz, G.E. Hilmas, J. Eur. Ceram. Soc. 29 (2009) 3401.
- [9] S. Zhu, W.G. Fahrenholtz, G.E. Hilmas, S.H. Zhang, Mater. Sci. Eng. A459 (2007) 167.
- [10] W.G. Fahrenholtz, G.E. Hilmas, S.C. Zhang, S. Zhu, J. Amer. Ceram. Soc. 91 (2008) 1398.
- [11] S.C. Zhang, G.E. Hilmas, W.G. Fahrenholtz, J. Amer. Ceram. Soc. 91 (2008) 3530.
- [12] K. Chenoweth, A.C.T. Van Duin, W.A. Goddard III, J. Phys. Chem. 112 (2008) 1040.
- [13] K.D. Nielson, A.C.T. Van Duin, J. Oxgaard, W.Q. Deng, W.A. Goddard III, J. Phys. Chem. 109 (2005) 493.
- [14] A.C.T. Van Duin, B.V. Merinov, S.S. Jang, W.A. Goddard III, J. Phys. Chem. A 112 (2008) 3133.
- [15] A.C.T. Van Duin, S. Dasgupta, F. Lorant, W.A. Goddard III, J. Phys. Chem. A 105 (2001) 9396.
- [16] ATK, Version 11.2.3, Quantum wise. (mai 2011) <<http://www.quantumwise.com>>.
- [17] I.R. Shein, A.L. Ivanovskii, J. Phys.: Condens. Matter 20 (2008) 415218.